Distal axonopathy with structural persistence in glaucomatous neurodegeneration

Samuel D. Crish[a], Rebecca M. Sappington[a], Denise M. Inman[b], Philip J. Horner[b], and David J. Calkins[a,1]

[a]The Vanderbilt Eye Institute and Vanderbilt Brain Institute, Vanderbilt University Medical Center, Nashville, TN 37232; and [b]Department of Neurosurgery, University of Washington, Seattle, WA 98104

Edited by John E. Dowling, Harvard University, Cambridge, MA, and approved February 1, 2010 (received for review November 16, 2009)

An early hallmark of neuronal degeneration is distal transport loss and axon pathology. Glaucoma involves the degeneration of retinal ganglion cell (RGC) neurons and their axons in the optic nerve. Here we show that, like other neurodegenerations, distal axon injury appears early in mouse glaucoma. Where RGC axons terminate in the superior colliculus, reduction of active transport follows a retinotopic pattern resembling glaucomatous vision loss. Like glaucoma, susceptibility to transport deficits increases with age and is not necessarily associated with elevated ocular pressure. Transport deficits progress distal-to-proximal, appearing in the colliculus first followed by more proximal secondary targets and then the optic tract. Transport persists through the optic nerve head before finally failing in the retina. Although axon degeneration also progresses distal-to-proximal, myelinated RGC axons and their presynaptic terminals persist in the colliculus well after transport fails. Thus, distal transport loss is predegenerative and may represent a therapeutic target.

axon transport | optic neuropathy | retinal ganglion cell | glaucoma | optic nerve

Glaucoma is an age-related disease of the visual system that will afflict 80 million people by 2020; it is the leading cause of irreversible blindness (1). Vision loss in glaucoma arises from the degeneration of retinal ganglion cell (RGC) neurons and their axons, which comprise the optic nerve (2, 3). As age is the leading risk factor, the only modifiable risk factor is elevated intraocular pressure (IOP) (4). RGC degeneration involves stressors at proximal locations both in the retina and optic nerve head, where RGC axons pass unmyelinated into the nerve. There, deprivation of trophic factors as a result of compromised axonal integrity and transport is thought to be integral (5–8). However, in other neurodegenerative diseases such as Alzheimer disease, Parkinson disease, and amyotrophic lateral sclerosis, neuronal stress at proximal sites manifests early as deficits in axonal transport and associated axonopathies at distal projections (9–11). As neurodegeneration in glaucoma shares several mechanistic commonalities with these disorders (12, 13), it is reasonable to question whether distal axon injury is also relevant.

Here we apply a well-characterized mouse model of glaucoma (DBA/2) and an acute model to probe the relevance of early distal axonopathy to RGC degeneration. DBA/2 mice present age-dependent elevations in IOP as a result of pigmentary dispersion in the anterior eye that are linked to RGC degeneration (14, 15). Retrograde transport from the SC persists as late as 18 months of age in the DBA/2 mouse (16, 17). Here we examine anterograde transport from the retina to the superior colliculus (SC), the primary projection site for RGCs in the rodent brain (18, 19). Disruption of transport in the brain is challenged even earlier and follows a spatial pattern similar to that of vision loss in glaucoma. Transport dysfunction proceeds from the SC to the optic nerve and retina and is accompanied by axonal dystrophies indicative of distal injury. Even after transport failure, key structures in the SC remain, including the myelinated axonal tract and the projection of RGC presynaptic terminals. Thus, preserving axonal transport during this period may represent an opportunity to reduce neurodegeneration in glaucoma.

Results

Distal Loss of Transport Is Retinotopic and Age-Dependent. RGC axons course through layer III of the SC to contact layer II neurons retinotopically (20). These can be visualized by intraocular injection of cholera toxin β-subunit (CTB), which labels the entire retinal projection via active uptake and transport (21, 22). For a 5-mo C57 and a 5-mo DBA/2, CTB labeled the entire retinotopic projection in the SC except for the retinal optic disk, which does not contain RGCs (Fig. 1 *A* and *B*). In contrast, the SC of an 8-mo DBA/2 demonstrated a focal deficit extending caudally from the optic disk gap (Fig. 1*C*), whereas a 10-mo DBA/2 SC contained a massive deficit that left the entire medial-caudal quadrant devoid of label (Fig. 1*D*).

The SC maps in Fig. 1 *C* and *D* resemble sectorial vision loss in glaucoma, which extends to the RGC-rich central retina (23). Some degenerative markers in the aged DBA/2 optic nerve and retina also have this pattern (8, 14, 24, 25). The area around the optic disk in the rodent contains the highest RGC density, like the human central retina (26). Whereas C57 mice showed no change in CTB label (Fig. 2*A*), label in DBA/2 SC ranged from complete to severely depleted from 3 to 10 mo (Fig. 2 *B–E*). Loss progressed either caudally or rostrally to adjoin a deficit near the optic disk (arrows in Fig. 2). An entire caudal or rostral sector was depleted before the opposing sector was affected (Fig. 2*E*). Label decreased steadily between 3 mo and 10 mo (Fig. 2*F*; $P < 0.001$). By 12 mo, only one of 10 SC had a small level of label (25%); at ≥15 mo, label was absent.

Loss of CTB label in the SC did not correlate with IOP (Fig. S1*A*). Like IOP, average intact label was similar between 3 mo and 5 mo ($P = 0.91$; Fig. S1*B*). Although IOP changed the most between 5 mo and 8 mo, CTB label was steady ($P = 0.17$) until decreasing by 96% between 8 mo and 12 mo ($P < 0.001$; Fig. S1*B*). This suggests that, although IOP cannot predict a deficit, aging can influence the likelihood of one for a given IOP. We tested this directly by comparing CTB in the SC of young (3–4 mo) and moderately aged (7–9 mo) rats with equivalent IOP elevations induced acutely (27). For both groups, injection of polystyrene microbeads into the aqueous chamber of the eye induced a 45% elevation in IOP compared with an equal volume of saline solution (Fig. 3*A*). After 2 weeks, CTB in the SC was unaffected in young animals, whereas aged animals exhibited a 60% reduction in the SC for the microbead-injected eye (Fig. 3 *B* and *C*; $P < 0.0001$). Like the DBA/2 mouse, a given IOP was more likely to induce transport loss in the SC of older animals.

Author contributions: S.D.C., R.M.S., D.M.I., P.J.H., and D.J.C. designed research; S.D.C., R.M.S., and D.M.I. performed research; S.D.C., R.M.S., D.M.I., and D.J.C. analyzed data; and S.D.C., R.M.S., and D.J.C. wrote the paper.

The authors declare no conflict of interest.

This article is a PNAS Direct Submission.

Freely available online through the PNAS open access option.

[1]To whom correspondence should be addressed. E-mail: david.j.calkins@vanderbilt.edu.

This article contains supporting information online at www.pnas.org/cgi/content/full/0913141107/DCSupplemental.

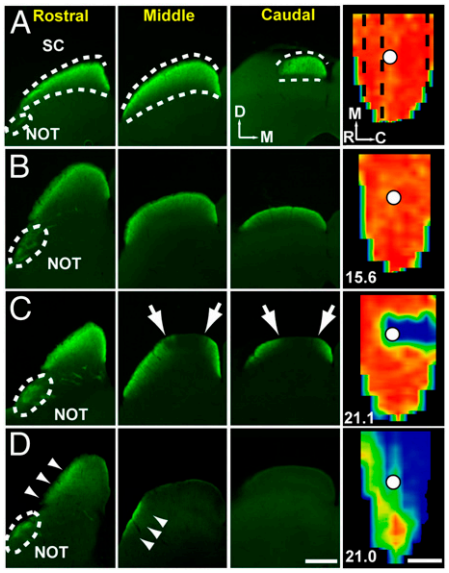

Fig. 1. Transport deficits in the DBA/2 SC. (*A*) Cross-sections through a 5-mo C57 brain showing normal RGC transport in the superficial SC (dotted lines) and in the nucleus of the optic tract (NOT) following unilateral injection of CTB (green). At far right is a complete retinotopic SC map with representation of optic disk gap (circle) and location of representative cross-sections (black dotted lines). Dorsal (D), rostral (R), caudal (C), and medial (M) are indicated. (*B*) SC of 5-mo DBA/2 with complete CTB label and corresponding retinotopic map. (*C*) SC of 8-mo DBA/2 with a 25% deficit in CTB middle to caudal (arrows) and resulting map. (*D*) SC from 10-mo DBA/2 with marginal retention of CTB label (arrowheads) shows an 88% retinotopic deficit. For DBA/2, IOP in mmHg is indicated for the corresponding eye. CTB signal density varies from 100% (red) to 50% (green) to 0% (blue). (Scale bars in *D*: 500 μm for sections or maps.)

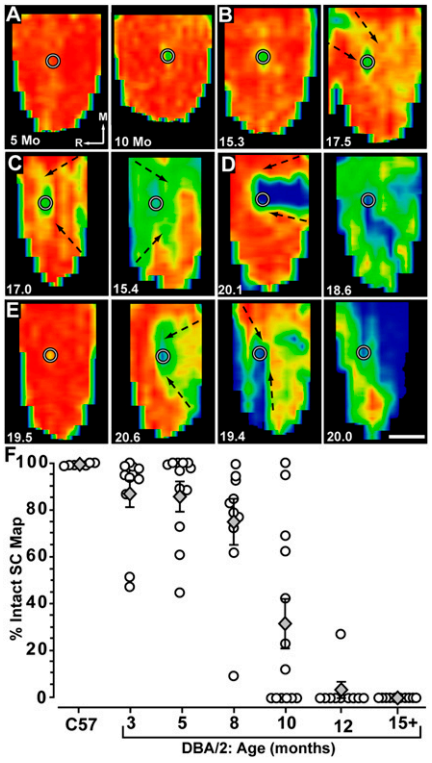

Fig. 2. Sectorial transport deficits. (*A*) Map of CTB in 5- and 10-mo C57 SC with optic disk gap (circle) and rostral (R) and medial (M) are indicated. CTB maps in DBA/2 SC for 3-mo (*B*), 5-mo (*C*), 8-mo (*D*), and 10-mo (*E*) mice with deficits progressing from rostral or caudal edge to the optic disk gap (arrows). IOP in mmHg is indicated. (Scale bar: 500 μm.) (*F*) Fraction of SC retinotopic map with ≥70% CTB signal density versus age for individual SC (open circles). Five- and 10-mo C57 SC shown in a single group ($n = 3$ each). Individual SC separated horizontally for clarity. Mean ± SE is shown (diamonds). DBA/2 transport differs from C57 at 8 mo ($P = 0.05$, $n = 10$), 10 mo ($P = 0.004$, $n = 13$), 12 mo ($P < 0.001$, $n = 10$), and ≥15 mo ($P < 0.001$), but not for 3 mo ($P = 0.13$, $n = 11$) or 5 mo ($P = 0.16$, $n = 12$). For ≥15 mo, $n = 16$ (all 0 signal), but only 10 points shown for clarity.

Transport Failure Progresses Distal to Proximal. The retinas projecting to DBA/2 SC with no CTB label nevertheless demonstrated pockets of intact physiological uptake in RGC cell bodies and transport in axons (Fig. 4). These were visualized by immunolabeling against either the cytoskeletal marker α-tubulin (Fig. 4 *A*–*C*) or phosphorylated heavy-chain neurofilaments (Fig. 4 *D*–*F*). Retinas projecting to SCs with intact label had more CTB-transporting RGCs than retinas serving SCs with depleted label (Fig. 4 *G* and *H*). However, when quantified, these did not correlate ($P = 0.17$; Fig. 4*I*). Even for blank SC, RGC uptake in each corresponding hemifield was considerable. Seven SC in Fig. 4*I* had collicular CTB in ≤45% of the retinal representation; of these, five had corresponding retina with both hemifields containing twice that level of labeled RGCs. Two 10-mo SC had the same level of signal (31%), but the corresponding retinal hemifields differed in uptake by 40% to 90%. Only one retina had a hemifield with less CTB uptake than SC label. Thus, the distal loss of CTB label cannot be explained patently by uptake failure. A small number of astrocytes in 12-mo retina contained CTB but did not stain for RGC markers.

RGCs also project to secondary sites in the brain that lie anterior to the SC (e.g., more proximal to the eye). These include the nucleus of the optic tract (see Fig. 1), the ventral lateral geniculate nuclei (LGN; vLGN) and dorsal LGN (dLGN), and the olivary pretectal nucleus (OPT), all of which derive input from collaterals of RGC axons projecting to the SC (18, 19, 28). In a 10-mo DBA/2 SC with full CTB (Fig. 5*A*), the v/dLGN and the OPT also demonstrated intact label. Even in SC completely devoid of transported CTB, some label persisted to the LGN and the OPT (Fig. 5 *B* and *C*) or just the OPT (Fig. 5*D*). In DBA/2 older than 12 mo ($n = 16$), no RGC projection site demonstrated CTB. However, some of these animals retained transported CTB in the optic tract and distal optic nerve; these were marked by axonal dystrophies with aggregating CTB (Fig. 5*E*). Even in a 12-mo animal with no transported CTB in the brain or optic tract, label clearly penetrated through the optic nerve head to the myelinated portion of the nerve itself and collected in axonal swellings similar to those in the optic tract (Fig. 5*F*). Of 14 animals at 10 to 12 mo with no CTB in the SC, six (43%) retained label in the optic projection up to the LGN or OPT, four (29%) up to the optic tract, three (21%) up to the optic nerve, and one (7%) did not exhibit any CTB outside of the retina (Fig. S2*A*). Thus, failure of CTB transport occurs first in the SC and then at more anterior sites in order of increasing proximity to the eye (Fig. S2*B*).

Distal Axonopathy with Structural Persistence. Transport failure often involves distal axonal dystrophies and "dying back" (11). Similar dystrophies contained CTB in the DBA/2 SC and in RGC axons labeled by antibodies against estrogen-related receptor–β (ERRβ), which mark the entire RGC projection (29) (Fig. S3). In our acute model (Fig. 3), progression of deficits in CTB transport and axonal dystrophies were similar to the DBA/2 (Fig. S4). To determine whether axon degeneration also progresses in a distal-to-proximal manner, we quantified degenerating profiles in the optic nerve at a proximal location near the nerve head (Fig. 6*A Left*) and more distally near the optic chiasm (Fig. 6*A Right*). Across ages, the number of degenerating profiles was always greater in the distal nerve (Fig. 6*B*). Whereas the number of degenerating profiles increased both distally and proximally with age, the ratio of distal to

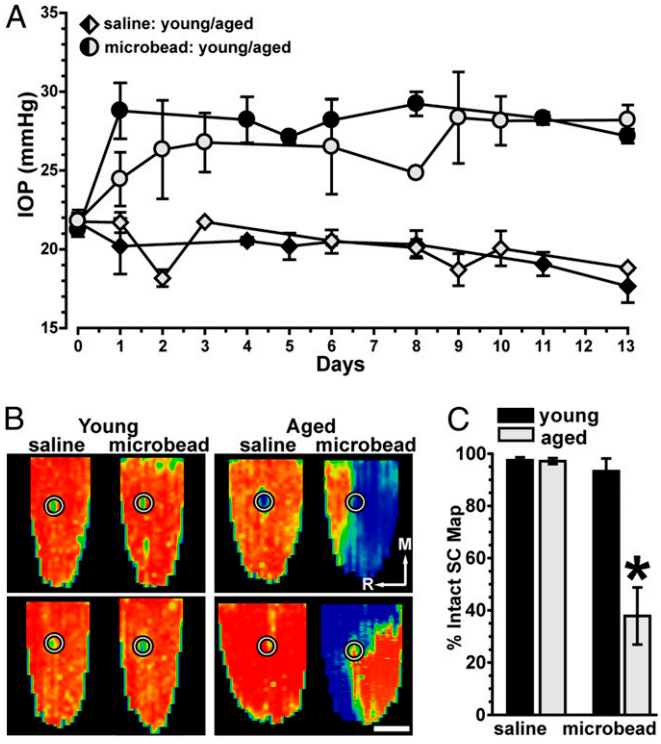

Fig. 3. Transport loss in acute glaucoma with age. (*A*) IOP in young (3–4 mo) and aged (7–9 mo) rats is elevated acutely by 40% to 45% with microbead injection (circles) compared with saline solution in the opposite eye (diamonds). IOP is the same for young and aged rats for both the saline ($P = 0.66$) and microbead ($P = 0.77$) eye, whereas the microbead-induced elevation was significant for both age groups ($P < 0.001$). (*B*) Maps of CTB label for two young rats (*Left*) were intact, whereas two aged rats (*Right*) had deficits for the microbead-injected eye of 80% and 60%, respectively. Rostral (R) and medial (M) are indicated. (*C*) Fraction of intact SC retinotopic map (≥70% CTB signal density) was reduced in aged ($P < 0.001$, $n = 5$) but not young ($P = 0.82$, $n = 5$) microbead-injected rats. (Scale bar in *B*: 500 μm.)

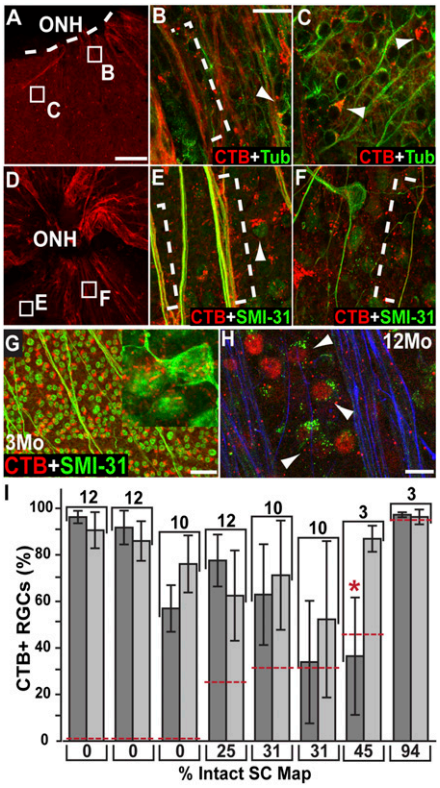

Fig. 4. Active uptake persists. (*A*) Twelve-month retina has some CTB+ axons (red) near optic nerve head (ONH). Corresponding SC contained no CTB signal. (*B* and *C*) Two locations from *A* labeled for α-tubulin (Tub). Region in *B* has both intact CTB transport (bracket) and uptake (arrowhead); region in *C* has only uptake (arrowheads). (*D*) Ten-month retina with residual CTB (red); SC contained none. (*E* and *F*) Two locations from *D* labeled for phosphorylated heavy-chain neurofilament (SMI-31). Region in *E* has both intact transport (brackets) and uptake (arrowhead); region in *F* shows a single transporting axon (bracket). (*G*) Five-month retina shows extensive CTB uptake in labeled RGCs. CTB is compartmentalized in the endoplasmic reticulum before transport and thus does not colocalize strictly with SMI-31 (*Inset*) (21). Green signal has been adjusted down to decrease background. (*H*) Brn3a-labeled RGCs (red) in a 12-mo retina contain CTB (green; arrowheads). Blue levels (SMI-31) adjusted to accent nontransporting axons. Brain contained no CTB. (*I*) RGCs with CTB uptake (%) versus fraction of intact SC map. Cells quantified in fields from the two hemiretinas (gray bars) in eight eyes (mean ± SD). Age (mo) and level of uptake required to match SC transport (dotted lines) are indicated. Asterisk marks only hemifield with uptake below transport. (Scale bars: 200 μm in *A* and *D*; 20 μm in *B*, *C*, and *E*–*G*; 5 μm in *H*.)

proximal profiles decreased (Fig. 6*C*). This is consistent with a distal-to-proximal progression.

Although increasing in number with age, degenerating axon profiles in the optic nerve were a small fraction of the total number of axons: only 3% to 7% at 13 mo. Even at this age, after anterograde transport of CTB fails (Fig. 2*F*), the number of intact axons ranged from 30% to 90% of the number for unaffected nerves (30). Levels of RGC axonal myelin in layer III were comparable between a 3-mo SC and an 18-mo SC (31) (Fig. 6*D*). When reconstructed from serial cross-sections, the volume of the superficial SC was nearly constant with age and across levels of intact CTB signal (Fig. 6*E*). For no age group did SC CTB level predict tissue volume (correlation coefficient ≤0.34, $P \geq 0.35$). The volume at 3 mo (0.54 ± 0.09 mm^3) was slightly higher than at 5 to 8 mo (0.48 ± 0.08 mm^3; $P = 0.05$). However, between 5–8 mo and 10–12 mo (0.46 ± 0.10 mm^3), there was no difference ($P = 0.44$) in volume despite a nearly fourfold difference in mean transport (80.2% ± 23.7 vs. 23.9% ± 34.7, respectively; $P < 0.001$). SC volume eventually diminished, shrinking considerably by 15 to 22 mo (0.32 ± 0.08 mm^3) compared with 10 to 12 mo ($P < 0.001$). Even so, some SC in this oldest group had normal volume (Fig. 6*E*).

Key structures in the RGC projection also persisted. In a 3-mo DBA/2 with full CTB in one SC and reduced CTB in the other, ERRβ labeling of RGC axon terminals in layer II was comparable (Fig. 7*A*). Similarly, in a 10-mo animal, ERRβ-labeled RGC axon terminals persisted throughout both SCs, although each had little CTB (Fig. 7*B*). Eventually ERRβ labeling of RGC axons diminished, following a distal-to-proximal progression. In a 17-mo animal with no CTB signal in the optic projection, ERRβ expression was present in RGC terminals of one SC and in both optic tracts (Fig. 7*C*). Antibodies against vesicular glutamate transporter 2 (VGluT2) selectively mark RGC synapses in layer II of the SC (32). VGluT2 label also persisted beyond CTB signal (Fig. 7 *D* and *E*). When quantified in serial sections, both ERRβ- and VGluT2-labeled RGC projections maintained nearly 100% representation regardless of CTB signal (Fig. 7*F*). Only for the very oldest animals without signal did these markers dissipate.

Discussion

Vision loss in glaucoma is sectorial, extending retinotopically to the RGC-rich central retina (23). This pattern is matched by pathologic process in the retina and optic nerve for both human glaucoma (33) and the DBA/2 mouse (8, 14, 24, 25). The depletion of CTB transport from the retina to its primary projection site, the SC, follows a

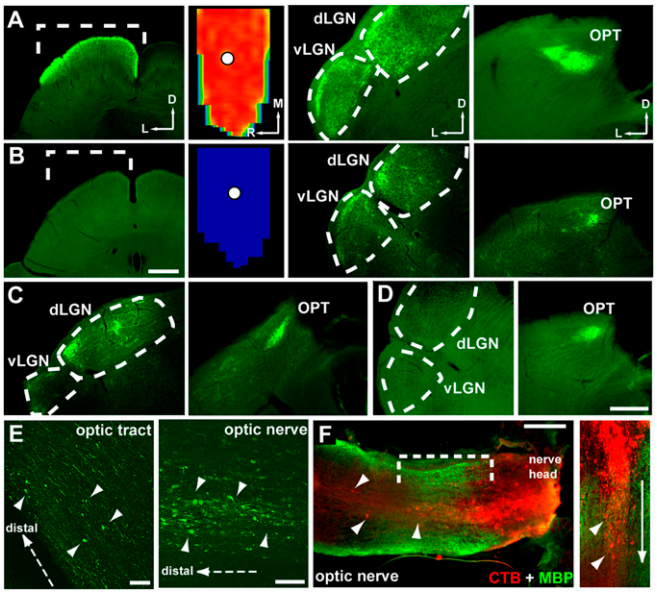

Fig. 5. Distal to proximal transport loss. (*A*) Ten-month SC section and complete retinotopic map with optic disk gap (circle). Ventral/dorsal LGN and OPT anterior to the SC with intact CTB. Lateral (L), medial (M), rostral (R), and dorsal (D) are indicated. (*B*) CTB absent in 10-mo SC but retained in LGN and OPT. (*C*) CTB present in dLGN and OPT but not vLGN of 10-mo brain with no SC signal. (*D*) A 12-mo brain with no signal in SC and LGN but some in OPT. (*E*) Optic tract and nerve from 10-mo brain with no signal shows CTB+ axonal dystrophies. Direction of axon terminals indicated (distal). (*F*) In 12-mo animal with no brain signal, CTB collects in axonal dystrophies (arrowheads) of optic nerve labeled for myelin basic protein (MBP) after penetrating beyond the unmyelinated nerve head. Bracketed region at higher magnification (*Right*) with dystrophic axons (arrowheads) extending toward the brain (arrow). (Scale bars: 500 μm in *B* and SC cross-section in *A*; 250 μm in *D* and LGN and OPT in *A*–*D*; 20 μm in *E*; and 200 μm in *F*.)

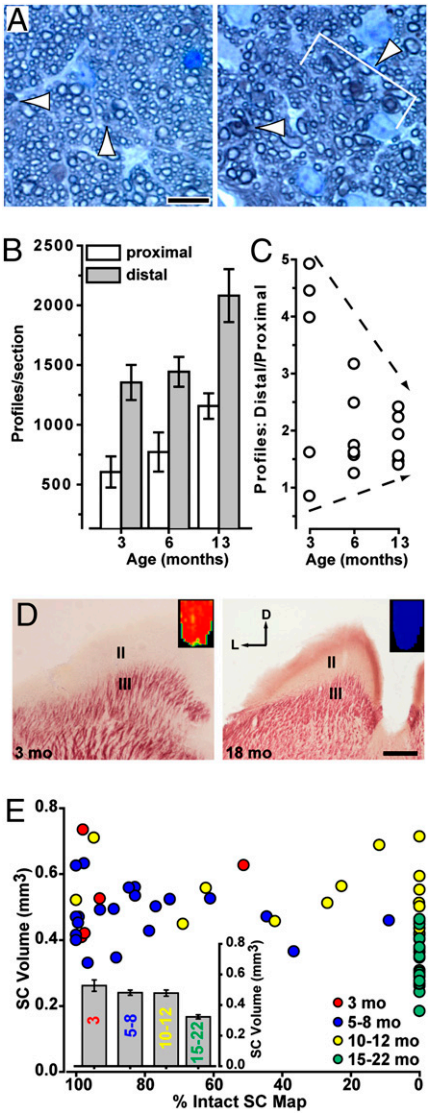

Fig. 6. Degeneration in the DBA/2. (*A*) Cross-sections through proximal (*Left*) and distal (*Right*) optic nerve of a 13-mo DBA/2 shows degenerating profiles (arrowheads, bracket). (*B*) Degenerating profiles per section for three ages (n = 5–6). (*C*) Ratio of distal to proximal degenerating profiles decreases with age. (*D*) Rostral SC from 3-mo (*Left*) and 18-mo (*Right*) DBA/2 mice show comparable Black Gold II–stained RGC axon myelin in layer III despite opposing fractions of intact SC map (*Insets*). Lateral (L) and dorsal (D) are indicated. (*E*) Volume of superficial SC reconstructed from serial sections changes very little across ages and range of intact CTB mapping. (*Inset*) Average SC volume across age groups. (Scale bars: 10 μm in *A*, 200 μm in *D*.)

similar retinotopic pattern for both the DBA/2 and older rats (Figs. 1–3). This is significant because the rim of the optic disk in the rodent contains the most RGCs, similar to the human central retina (26). Elevated IOP is a major risk, but approximately 50% of glaucoma begins without it (34). Age is the greatest risk factor (4) and influences transport loss in the DBA/2 SC (Fig. 2); deficits were associated with lower IOP as age increased (Fig. S1). In our acute model (30), an identical IOP elevation caused a transport deficit in older but not younger animals (Fig. 3). Thus, sensitivity to IOP is an added stressor to other age-related factors (35). A small number of younger DBA/2 (3–5 mo) had transport deficits without IOP elevation (Fig. 2), so additional pathogenic mechanisms must be at work early (30, 36). Retrograde transport from the SC to the retina in the DBA/2 is maintained at 20% to 30% capacity up to 18 mo of age (16, 17). Anterograde transport is challenged considerably earlier, with complete failure to the SC at 11 to 12 mo and to all RGC targets in the brain after 12 mo (Figs. 2 and 5).

Transport loss appears first at its most distal site, where RGC axons terminate in the SC. Deficits progress to more anterior RGC brain targets, to the optic tract and nerve, and finally to the retina, where active uptake eventually fails (Figs. 4 and 5). Even in 10- to 12-mo DBA/2 with no SC transport uptake persists, although it is highly variable (Fig. 4*I*), like other features in the DBA/2 (14, 30). Even when absent in the brain, residual transport along individual axons can penetrate through the optic nerve head before dissipating in the nerve itself (Fig. 5*F*; also see ref. 14). We found that the distal optic nerve of the DBA/2 degenerates before the proximal nerve, but at a modest level after transport depletion (Fig. 6 *B* and *C*). Thus, RGC degeneration appears to be asymmetric from neuron to neuron after transport is lost, and is much slower.

Downstream apoptotic mechanisms contribute late in glaucoma (25, 37, 38), and axonal pathology precedes somatic degeneration (14–16, 24, 39, 40). Early distal transport deficits and axonal dystrophies are relevant in Alzheimer disease, Parkinson disease, and amyotrophic lateral sclerosis (9–11). Distal sites within the optic pathway of the DBA/2 also demonstrate axonal dystrophies (Fig. S3); these are indicative of local blockade of cytoskeletal, metabolic, or synaptic components (41). In acute glaucoma models, RGC targets in the brain demonstrate atrophy associated with loss of recipient neurons (42). DBA/2 glaucoma is generally progressive, and the SC retains most of its volume after transport loss (Fig. 6*E*). Similarly, RGC axons, terminals, and synaptic markers persist in the SC after transport has failed (Fig. 7). This is consistent with findings of a considerable number of surviving axons in older optic

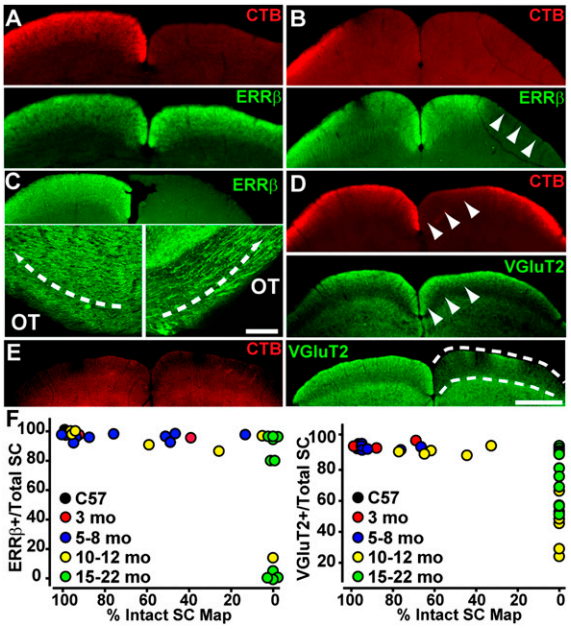

Fig. 7. Structural persistence after transport loss in DBA/2. (*A*) Three-month SC after bilateral CTB injection shows signal on one side with a deficit on the other (*Upper*). ERRβ labeling of RGC axon terminals in same section persists on both sides (*Lower*). (*B*) Ten-month left and right SC with severe loss of CTB signal (*Upper*) shows ERRβ beginning to dissipate (*Lower*), especially on side with no signal (arrowheads). (*C*) Seventeen-month left and right SC with ERRβ-labeled RGC axon terminals on one but not the other side (*Upper*). ERRβ-labeled RGC axons persist in optic tract (OT) for both (*Lower*). Arrows show direction of terminals. (*D*) Section of 8-mo SC with modest CTB signal deficit on right (arrowheads, *Upper*) shows full complement of RGC presynaptic terminals labeled for VGluT2. (*E*) Eighteen-month SC with complete bilateral loss of signal (*Left*). VGluT2-labeled RGC terminals persist on the left but not the right (dashed lines). (*F*) Fraction of SC volume with intact ERRβ label persists across ages even with severely depleted CTB signal maps (*Left*), as does the fraction containing intact VGluT2. (Scale bars: 500 μm in *E* and in SC sections; 50 μm in *C* and in OT.)

nerves, even with diminished physiological activity (Fig. 6*B*) (14, 17, 36).

Our results do not address the site of axonal insult, but demonstrate that distal transport depletion is an early manifestation. An important hypothesis in glaucoma posits trophic deprivation proximally at the optic nerve head along with loss of axonal integrity (5–8, 43). Myriad somatic and dendritic factors are also likely to contribute, including intrinsic pressure sensitivity and synapse elimination (35, 44). Importantly, transport loss at distal sites is predegenerative in that much of the structure of the retinal projection remains intact for a period afterward. Thus, early vision loss in glaucoma could be abated by interventions that preserve distal axonal function before the loss of the neuronal substrate.

Methods

Animals. All experimental procedures were approved by the Vanderbilt University Medical Center Institutional Animal Care and Use Committee. DBA/2 and C57BL/6 mice were obtained from Jackson Laboratories and Brown Norway rats from Charles River. Animals were maintained in a 12-h light/dark cycle with standard rodent chow available ad libitum as described (27, 30). For acute elevation of IOP, we used microbead occlusion of aqueous flow as described (27). IOP was measured in a subset of DBA/2 mice and in awake rats using the Tono-Pen XL (Medtronic Solan) as described previously (27, 30).

Anterograde Transport Measurement. We used 2.5% isoflurane anesthesia for intravitreal injection of 1 μL (mice) or 2 μL (rats) of CTB conjugated to Alexa Fluor–488 or -594 (1 μL of 1% CTB in sterile PBS solution; Invitrogen) using a glass pipette (50-μm tip). CTB is an established marker for active uptake and transport and has been used successfully to assess the retinal projection to the SC in injury (21, 22, 45). Animals were transcardially perfused with 4% paraformaldehyde in PBS solution and tissues removed after 48 h of CTB activity, an established period for complete retinotopic mapping of the SC for mice and other small mammals (28). CTB signal in serial coronal brain sections (50 μm) was photographed digitally on an Olympus AX-70 microscope. Tissues were processed for immunocytochemistry as described in the subsequent sections.

We quantified CTB signal density in the SC using ImagePro (Media Cybernetics). Background intensity for each brain section was set independently for normalization using pixel strength of the nonretinorecipient SC (layers IV–VII) and the periaqueductal gray. Using layer IV as the ventral border, we outlined in each section the boundaries of the superficial SC (19, 20), which was partitioned into 6-μm bins from medial to lateral. For each bin, the area of pixels with CTB signal above background was divided by total pixel area to determine CTB density. This was assigned a colorimetric representation ranging from 0% (blue) to 100% (red) at each mediolateral location in the SC section. Using section thickness and intersection distance, we adjoined sections to construct a colorimetric representation of CTB density across the retinotopic SC map. For each SC, we determined the fraction of intact retinotopic map, defined as the percent area with CTB signal ≥70% density. Some images have had the background signal increased to enhance visibility of key structures in the optic projections; this did not affect identification and quantification of CTB given the normalized algorithm described.

Immunocytochemistry and Histology. Labeling of the retina in whole-mount preparations, sections of optic nerve, and brain was performed as previously described (35). We used antibodies against detyrosinated α-tubulin (monoclonal, 1:200; Millipore) and phosphorylated heavy-chain neurofilament (SMI31, 1:1,000; Sternberger Monoclonal) (8, 15) to visualize RGCs; myelin basic protein (SMI99, 1:1,000; Sternberger Monoclonal) to delineate the optic nerve head; ERRβ (polyclonal, 1:500; Sigma) (29) to label the RGC SC projection; hyperphosphorylated heavy-chain neurofilament (SMI34, 1:1.000; Sternberger Monoclonal) (15) to highlight axonal dystrophies; and VGluT2 (polyclonal, 1:500; Synaptic Systems) (32) to visualize RGC axon terminals in the SC. We used Alexa Fluor– (Invitrogen) or Cy5- (Jackson ImmunoResearch) conjugated secondary antibodies (1:200). Confocal images were taken using a Zeiss LSM510 Meta upright confocal microscope and an Olympus FV-1000 inverted confocal microscope. VGluT2- and ERRβ immunolabeling in the SC was quantified using the same process described here for quantifying CTB density. To visualize RGC axons in layer III of the SC and determine SC volume, we used the myelin marker Black Gold II (Histochem) (31) in serial 50-μm SC sections. For quantifying axons in the optic nerve, segments near the eye (proximal) and optic chiasm (distal) were quantified as described (16, 30). For scoring RGCs containing CTB, retinas were sampled in confocal micrographs using a grid with 318 × 318-μm fields every 636 μm. SMI31+ and CTB+ cell bodies were counted by two independent raters across the entire retina.

ACKNOWLEDGMENTS. Confocal imagery was performed through the Vanderbilt University Medical Center Cell Imaging Shared Resource core facility. This work was supported by the Glaucoma Research Foundation (D.J.C. and P.J.H), an Unrestricted Departmental Grant from Research to Prevent Blindness (D.J.C.), American Health Assistance Foundation (D.J.C.), Vanderbilt Discovery grants (D.J.C.), National Institutes of Health Grant EY017427 (to D.J.C.), Vanderbilt Vision Research Center Core Grant 5P30EY008126-19, and fellowships from Fight for Sight (R.M.S., S.D.C.).

1. Quigley HA, Broman AT (2006) The number of people with glaucoma worldwide in 2010 and 2020. *Br J Ophthalmol* 90:262–267.
2. Quigley HA (1999) Neuronal death in glaucoma. *Prog Retin Eye Res* 18:39–57.
3. Nickells RW (2007) From ocular hypertension to ganglion cell death: a theoretical sequence of events leading to glaucoma. *Can J Ophthalmol* 42:278–287.
4. Heijl A, et al.; Early Manifest Glaucoma Trial Group (2002) Reduction of intraocular pressure and glaucoma progression: results from the Early Manifest Glaucoma Trial. *Arch Ophthalmol* 120:1268–1279.
5. Pease ME, McKinnon SJ, Quigley HA, Kerrigan-Baumrind LA, Zack DJ (2000) Obstructed axonal transport of BDNF and its receptor TrkB in experimental glaucoma. *Invest Ophthalmol Vis Sci* 41:764–774.
6. Quigley HA, et al. (2000) Retrograde axonal transport of BDNF in retinal ganglion cells is blocked by acute IOP elevation in rats. *Invest Ophthalmol Vis Sci* 41:3460–3466.
7. Martin KR, Quigley HA, Valenta D, Kielczewski J, Pease ME (2006) Optic nerve dynein motor protein distribution changes with intraocular pressure elevation in a rat model of glaucoma. *Exp Eye Res* 83:255–262.

8. Soto I, et al. (2008) Retinal ganglion cells downregulate gene expression and lose their axons within the optic nerve head in a mouse glaucoma model. *J Neurosci* 28: 548–561.
9. Fischer LR, et al. (2004) Amyotrophic lateral sclerosis is a distal axonopathy: evidence in mice and man. *Exp Neurol* 185:232–240.
10. Stokin GB, et al. (2005) Axonopathy and transport deficits early in the pathogenesis of Alzheimer's disease. *Science* 307:1282–1288.
11. Coleman M (2005) Axon degeneration mechanisms: commonality amid diversity. *Nat Rev Neurosci* 6:889–898.
12. McKinnon SJ (2003) Glaucoma: ocular Alzheimer's disease? *Front Biosci* 8:s1140–s1156.
13. Guo L, et al. (2007) Targeting amyloid-beta in glaucoma treatment. *Proc Natl Acad Sci USA* 104:13444–13449.
14. Schlamp CL, Li Y, Dietz JA, Janssen KT, Nickells RW (2006) Progressive ganglion cell loss and optic nerve degeneration in DBA/2J mice is variable and asymmetric. *BMC Neurosci* 7:66.
15. Howell GR, et al. (2007) Axons of retinal ganglion cells are insulted in the optic nerve early in DBA/2J glaucoma. *J Cell Biol* 179:1523–1537.
16. Buckingham BP, et al. (2008) Progressive ganglion cell degeneration precedes neuronal loss in a mouse model of glaucoma. *J Neurosci* 28:2735–2744.
17. Danias J, et al. (2003) Quantitative analysis of retinal ganglion cell (RGC) loss in aging DBA/2NNia glaucomatous mice: comparison with RGC loss in aging C57/BL6 mice. *Invest Ophthalmol Vis Sci* 44:5151–5162.
18. Linden R, Perry VH (1983) Massive retinotectal projection in rats. *Brain Res* 272: 145–149.
19. Hofbauer A, Dräger UC (1985) Depth segregation of retinal ganglion cells projecting to mouse superior colliculus. *J Comp Neurol* 234:465–474.
20. Dräger UC, Hubel DH (1976) Topography of visual and somatosensory projections to mouse superior colliculus. *J Neurophysiol* 39:91–101.
21. Angelucci A, Clascá F, Sur M (1996) Anterograde axonal tracing with the subunit B of cholera toxin: a highly sensitive immunohistochemical protocol for revealing fine axonal morphology in adult and neonatal brains. *J Neurosci Methods* 65:101–112.
22. Avilés-Trigueros M, et al. (2003) Transient ischemia of the retina results in massive degeneration of the retinotectal projection: long-term neuroprotection with brimonidine. *Exp Neurol* 184:767–777.
23. Goldblum D, Mittag T (2002) Prospects for relevant glaucoma models with retinal ganglion cell damage in the rodent eye. *Vision Res* 42:471–478.
24. Jakobs TC, Libby RT, Ben Y, John SW, Masland RH (2005) Retinal ganglion cell degeneration is topological but not cell type specific in DBA/2J mice. *J Cell Biol* 171: 313–325.
25. Reichstein D, Ren L, Filippopoulos T, Mittag T, Danias J (2007) Apoptotic retinal ganglion cell death in the DBA/2 mouse model of glaucoma. *Exp Eye Res* 84:13–21.
26. Dräger UC, Olsen JF (1981) Ganglion cell distribution in the retina of the mouse. *Invest Ophthalmol Vis Sci* 20:285–293.
27. Sappington RM, Carlson BJ, Crish SD, Calkins DJ (2010) The microbead occlusion model: a paradigm for induced ocular hypertension in rats and mice. *Invest Ophthalmol Vis Sci* 51: 207–216.
28. Crish SD, Dengler-Crish CM, Catania KC (2003) Central visual system of the naked mole-rat (Heterocephalus glaber). *Anat Rec A Discov Mol Cell Evol Biol* 288:205–212.
29. Real MA, Heredia R, Dávila JC, Guirado S (2008) Efferent retinal projections visualized by immunohistochemical detection of the estrogen-related receptor beta in the postnatal and adult mouse brain. *Neurosci Lett* 438:48–53.
30. Inman DM, Sappington RM, Horner PJ, Calkins DJ (2006) Quantitative correlation of optic nerve pathology with ocular pressure and corneal thickness in the DBA/2 mouse model of glaucoma. *Invest Ophthalmol Vis Sci* 47:986–996.
31. Schmued L, et al. (2008) Introducing Black-Gold II, a highly soluble gold phosphate complex with several unique advantages for the histochemical localization of myelin. *Brain Res* 1229:210–217.
32. Fujiyama F, et al. (2003) Changes of immunocytochemical localization of vesicular glutamate transporters in the rat visual system after the retinofugal denervation. *J Comp Neurol* 465:234–249.
33. Lei Y, et al. (2009) Topography of neuron loss in the retinal ganglion cell layer in human glaucoma. *Br J Ophthalmol* 93:1676–1679.
34. Shields MB (2008) Normal-tension glaucoma: is it different from primary open-angle glaucoma? *Curr Opin Ophthalmol* 19:85–88.
35. Sappington RM, Sidorova T, Long DJ, Calkins DJ (2009) TRPV1: contribution to retinal ganglion cell apoptosis and increased intracellular Ca2+ with exposure to hydrostatic pressure. *Invest Ophthalmol Vis Sci* 50:717–728.
36. Saleh M, Nagaraju M, Porciatti V (2007) Longitudinal evaluation of retinal ganglion cell function and IOP in the DBA/2J mouse model of glaucoma. *Invest Ophthalmol Vis Sci* 48:4564–4572.
37. McKinnon SJ, et al. (2002) Caspase activation and amyloid precursor protein cleavage in rat ocular hypertension. *Invest Ophthalmol Vis Sci* 43:1077–1087.
38. Huang W, et al. (2005) Transcriptional up-regulation and activation of initiating caspases in experimental glaucoma. *Am J Pathol* 167:673–681.
39. Libby RT, et al. (2005) Susceptibility to neurodegeneration in a glaucoma is modified by Bax gene dosage. *PLoS Genet* 1:17–26.
40. Whitmore AV, Libby RT, John SW (2005) Glaucoma: thinking in new ways-a rôle for autonomous axonal self-destruction and other compartmentalised processes? *Prog Retin Eye Res* 24:639–662.
41. Morgan JE (2004) Circulation and axonal transport in the optic nerve. *Eye (Lond)* 18: 1089–1095.
42. Weber AJ, Chen H, Hubbard WC, Kaufman PL (2000) Experimental glaucoma and cell size, density, and number in the primate lateral geniculate nucleus. *Invest Ophthalmol Vis Sci* 41:1370–1379.
43. Nakazawa T, et al. (2006) Tumor necrosis factor-alpha mediates oligodendrocyte death and delayed retinal ganglion cell loss in a mouse model of glaucoma. *J Neurosci* 26:12633–12641.
44. Stevens B, et al. (2007) The classical complement cascade mediates CNS synapse elimination. *Cell* 131:1164–1178.
45. Drouyer E, et al. (2008) Glaucoma alters the circadian timing system. *PLoS One* 3: e3931.